Journal of Environmental Chemical Engineering 8 (2020) 103756

Contents lists available at ScienceDirect

Journal of Environmental Chemical Engineering

journal homepage: www.elsevier.com/locate/jece

Mechanistic model of electrocoagulation process for treating vinasse waste: Effect of initial pH

Iqbal Syaichurrozi[a,b], Sarto Sarto[a,*], Wahyudi Budi Sediawan[a], Muslikhin Hidayat[a]

[a] Department of Chemical Engineering, Faculty of Engineering, Universitas Gadjah Mada, Jl. Grafika No.2, Yogyakarta, 55281, Indonesia
[b] Department of Chemical Engineering, Faculty of Engineering, University of Sultan Ageng Tirtayasa, Jl. Jendral Soedirman Km 3, Cilegon, 42435, Indonesia

ARTICLE INFO

Keywords:
Electrocoagulation
Initial pH
Mechanistic model
Vinasse
Waste

ABSTRACT

Electrocoagulation (EC) is widely applied to treat wastewaters. Vinasse is a bioethanol waste containing high Chemical Oxygen Demand (COD) and having low power Hydrogen (pH) level. Application of EC for treating vinasse has been studied by other authors, but development of mechanistic models has not been conducted yet. Because of the complex reactions in EC, building a mechanistic model is very interesting. The effect of initial pH in EC on COD removal of the vinasse was investigated and then the measured data was modeled. In the model, reactions in EC process consisted of adsorption, flocculation, entrapment, sedimentation and flotation. Measured data obtained through experiment included COD, total dissolved Fe, scum and sludge per real time during EC process. Increase in initial pH from 4.35 to 6.00 increased the kinetic constants of k_1 (adsorption), k_e (entrapment) and k_{sc} (flotation). Furthermore, some mathematical equations between the initial pH and the kinetic constants were successfully founded so that the EC performance for other initial pH (in range of 4.35–6.00) could be predicted. Meanwhile, ratio between removed COD to total operating cost for initial pH of 4.35, 5.00 and 6.00 after EC process for 60 min was 0.0570, 0.0506 and 0.0636 g-COD IDR^{-1} respectively.

1. Introduction

At the moment, bioethanol production in Indonesia is as much as 450 million liter per year [1]. Because the government has a target to replace fossil fuels need from 8 % (the year of 2013) to 31 % (the year of 2050) with renewable energy [2], the bioethanol production will increase significantly in the future. Unfortunately, to produce 1 L bioethanol, the industries generate 8 − 15 L vinasse waste [3]. The waste is a bottom product of distillation unit. It has very acidic level (pH of 3.75–4.5, [4,5]), contains high organic compound (Chemical Oxygen Demand (COD) more than 100,000 mg L^{-1}, [3,6]) and has high COD to Nitrogen (COD/N) ratio (approximately 205 [3]). According to Budiyono et al. [7], vinasse has to be treated to decrease the COD content before it is discharged to the water bodies. Nowadays, many methods can be utilized to decrease pollutants in wastewaters such as biological, physical, chemical and physicochemical treatments.

In biological treatments, Sepehri and Sarrafzadeh [8] proposed a nitrifying-enriched activated sludge (NAS) to improve filterability in membrane bioreactors in term of removing pollutants in synthetic wastewater. This concept was effective to be applied to wastewaters having low ratio of carbon to nitrogen (C/N). At low C/N ratio, nitrifying bacteria grew well which was 10 times more than that at high C/N ratio. It resulted high nitrification efficiency. Furthermore, Sapehri et al. [9] proposed collaboration between *Chlorella vulgaris* and NAS to remove pollutants in wastewaters. It increased nutrient removal and dissolved carbon capture. However, it was effective to be applied at low COD/N ratio because the growth rate of algae decreased at high COD/N ratio. Because vinasse contains high COD/N ratio (or C/N), the methods of NAS or algae-NAS are not suitable to be applied to treat the vinasse. In addition, the very high COD concentration, the biological treatment was not effective.

In chemical treatments, the catalytic degradation can be utilized to decrease pollutant concentration in wastewaters. Some metal and metal oxide nanoparticles (silver, platinum, gold, palladium, bimetallic composites) can be applied as nano-catalyst. However, in solution, they have a tendency to aggregate because of interparticle interactions via van der Waals forces and high surface energies [10]. That phenomenon will decrease the catalytic efficiency and stability. Hence, other components are needed to support the nanoparticles [10]. Zeng et al. [11] has successfully fabricated the novel MoS_2-PDA-Ag nanocomposites via mussel-inspired chemistry and then applied them as heterogeneous catalyst to remove 4-nitrophenol through microwave irradiation. However, catalytic degradation method is not more effective than adsorption method. The latter has easier operation and lower cost [12].

* Corresponding author.
E-mail address: sarto@ugm.ac.id (S. Sarto).

https://doi.org/10.1016/j.jece.2020.103756
Received 29 October 2019; Received in revised form 2 February 2020; Accepted 5 February 2020
Available online 06 February 2020

Nomenclatures

$[Fe^{2+}]$	Concentration of Fe^{2+} (g L^{-1})	M_w	Molar mass of Fe (56 g mol^{-1})
$[COD]$	Concentration of COD (g L^{-1})	z	Number of electron transfer (2 or 3)
$[Scum]$	Concentration of scum (g L^{-1})	F	Faraday's constant (96,500 C mol^{-1})
$[Sludge]$	Concentration of sludge (g L^{-1})	k_1	Reaction rate constant for adsorption (L g^{-1} sec^{-1})
$[A]$	Concentration of small aggregate (g L^{-1})	k_2	Reaction rate constant for flocculation (L g^{-1} sec^{-1})
$[A_2]$	Concentration of big aggregate (g L^{-1})	k_a	Reaction rate constant for oxidation at anode (sec^{-1})
d	Distance of electrodes (cm)	k_c	Reaction rate constant for reduction at cathode (sec^{-1})
e^-	Electron	k_e	Reaction rate constant for entrapment (sec^{-1})
I	Current (Ampere)	k_{sc}	Reaction rate constant for flotation (sec^{-1})
J	Current density (Ampere cm^{-2})	k_{sl}	Reaction rate constant for sedimentation (sec^{-1})
A_s	Active surface of electrode (cm^2)	EnC	Energy consumption (Ws L^{-1})
t	Electrolysis time (sec)	ElC	Electrode consumption (g L^{-1})
v	Volume of wastewater (L)	ChC	Chemical consumption (kg L^{-1})
		V	Voltage (Volt)
		κ	Conductivity (μS cm^{-1})

In physical treatments, some authors found that modified materials, as adsorbent, are effective to adsorb the specific pollutants. The mussel-inspired chemistry has been widely utilized for the fabrication of functional composites for catalytic degradation [10], environmental adsorption [10] and drug delivery application [13]. The mussel adhesive protein in mussel mucus corresponds to the strong adhesion of the mussel. The key component of it is the 3,4-dihydroxy-L-phenylalanine (DOPA). Furthermore, dopamine (DA) is one of DOPA derivative and polydopamine (PDA) is self-polymerization of DA [10]. The PDA nanoparticles could be used as an adsorbent for Copper (II) (Cu^{2+}) [12]. To increase an adsorption capacity, the PDA and DOPA with other components are used to make the novel composites that are used as adsorbents. The polyacrylamide immobilized molybdenum disulfide (MoS_2@PDA@PAM composites) [14], the carbon nanotubes based carboxymethyl chitosan nanocomposites (CNT-PDA-CS nanocomposites) [15], the functionalized carbon nanotubes with polydopamine and polyethylene polyamine (CNTs-PDA-PP) [16] showed satisfied results in Cu^{2+} removal by adsorption method. Furthermore, the functionalized SiO_2 nanoparticles with cationic polymers poly-((3-Acrylamidopropyl)trimethylammonium chloride) (SiO_2-PDA-PAPTCl) [17] and the functionalized Molybdenum disulfide with self-polymerization of levodopa (MoS_2-PDOPA polymer) [18] could remove organic dye.

The other materials such as the polyethylene polyamine@tannic acid encapsulated MgAl-layered double hydroxide (LDH-PP@TA) [19], the polyacrylamide immobilized molybdenum disulfide (GO-Fe_3O_4 composites) [20] and the polyethylenimine-tannins coated SiO_2 (SiO_2@PEI-TA) hybrid materials [21] also could adsorb Cu^{2+}. Meanwhile, the functionalized carbon nanotubes with tannins (CNT-TA) [22] and the sulfonic groups functionalized Mxenes (Ti_3C_2–SO_3H) [23] could remove methylene blue. Adsorption is effective for low pollutant concentration not for high pollutant concentration because it needs so many adsorbents for high pollutant concentration.

In physicochemical treatment, one of potential methods to treat vinasse is electrocoagulation (EC). Many authors reported that the COD in vinasse was successfully decreased through EC [24–29]. Application of EC for treating wastewaters is very attracting because of its advantages i,e simple equipment, easy operation, rapid sedimentation rate, low capital and operating cost, shortened retention period and very efficient in COD removal [30–34]. The main process for COD removal in EC is adsorption by coagulants of $Fe(OH)_2$ and $Fe(OH)_3$. The EC may be more efficient than adsorption by using adsorbents (previous paragraph), because the coagulants (such as $Fe(OH)_2$ and $Fe(OH)_3$) are continuously produced due to electrical force during EC process.

EC uses metals as electrodes. Anode and cathode are electrodes connected to positive and negative poles of power Direct Current (DC) supply. The electrodes are immersed in wastewaters. Iron (Fe) is a common metal used as electrode in this method. Meanwhile, contaminant removal efficiency was obtained higher by using Fe electrode

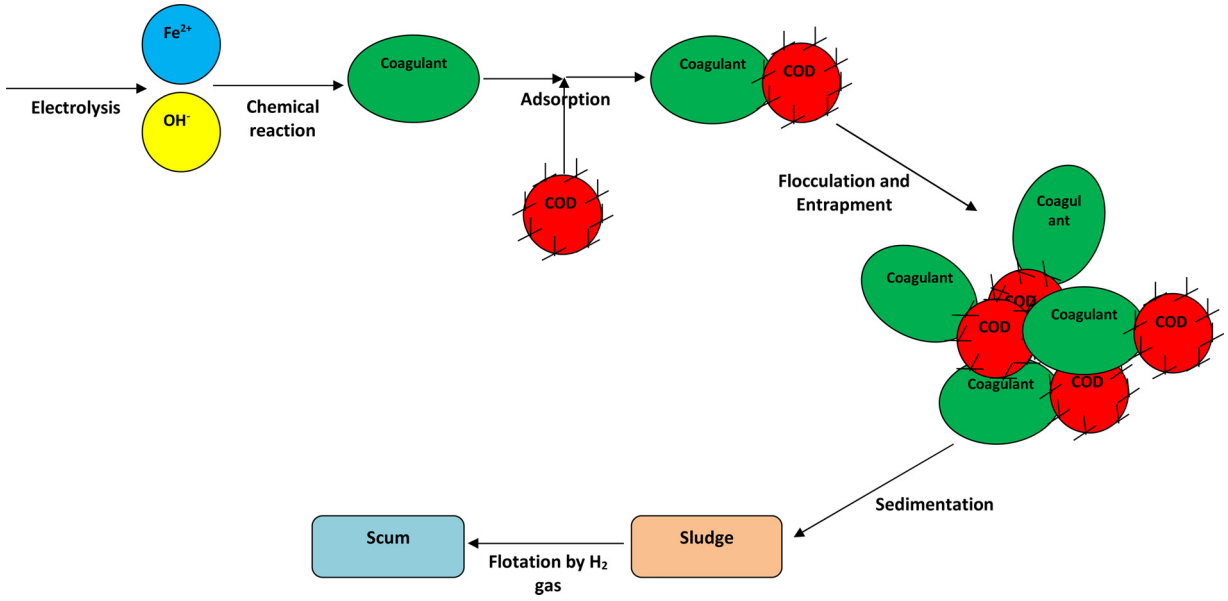

Fig. 1. Mechanism process during EC.

than by using Al electrode [35,36]. When a current is flowing, sacrificial anode (Fe) is dissolved to be Fe^{2+} ion. Meanwhile, the H_2O is to be H_2 gas and OH^- ion. Furthermore, Fe^{2+} is hydrolyzed to be coagulant of $Fe(OH)_2$ and $Fe(OH)_3$. The coagulants will adsorb the pollutants, hence favoring the formation of aggregates. The aggregates react each other to make the bigger aggregate via flocculation. The aggregates can be removed by sedimentation as sludge and by flotation as scum by evolved H_2 [37,38].

Degradation of pollutants during EC can be modeled by using adsorption kinetic models (empirical models) such as pseudo first order model, pseudo second order model, Langmuir model, Elovich model and fractional power model [39,40]. These models are used with assuming that the adsorption is limiting step in EC. However, it is very interesting to see the complex mechanism processes during EC. Thus, a mechanistic model has to be built to describe step by step of reactions in EC process. Based on our study of literatures, however, at the moment, there is no mechanistic model for EC, especially in term of vinasse treatment. Hence, this study proposed a novel mechanistic model that is new and original. For kinetic analysis using the mechanistic model, the experimental data was obtained from EC of vinasse at variation of initial pH.

Initial pH is one of the most factors affecting the pollutant removal. It is more important than current density [41]. According to Demirbas and Kobya [30], by using Fe electrode, initial pH of 6–7 resulted the more COD removal efficiency than the others with range of 3-8. Furthermore, Olya and Pirkarami [42] reported that the optimum initial pH in organic contaminant removal by using Fe-Fe electrode was 6. In this study, vinasse has low pH level (pH of 4.35, see point of 4.1). Therefore, this study varied the initial pH of vinasse to be 4.35, 5.00 and 6.00 by using NaOH. The neutral condition (pH of 7) was not conducted because it might result the almost same COD removal efficiency with pH of 6. Alkaline condition (pH of 8–14) was not conducted because it needs much more NaOH addition but the COD removal is low.

The mechanistic model contains some kinetic constants presenting the phenomena during EC process. For fitting between measured and predicted data, the kinetic constants have to be searched until the fitting error value is low. Furthermore, the mathematical correlation between the initial pH (4.35, 5.00, 6.00) and the kinetic constants would be built, so that the EC performance for other initial pH with range 4.35–6.00 could be predicted.

2. Mechanism of EC process

As illustration, Fig. 1 shows the mechanisms during EC. In this study, all processes are assumed to be irreversible process. Furthermore, decrease in wastewater volume during EC is ignored, so the volume is assumed to be constant. When iron is used as sacrificial anode in EC, Fe^{2+} ion is dissolved in the wastewater by the oxidation reaction at the anode (Eq. (1), [37]).

$$Fe \xrightarrow{k_a} Fe^{2+} + 2e^- \tag{1}$$

Meanwhile, OH^- ion and H_2 gas are resulted by water reduction reaction at the cathode (Eq. (2), [37]).

$$2H_2O + 2e^- \xrightarrow{k_c} H_2 + 2OH^- \tag{2}$$

Accumulation of OH^- ion increases the solution pH. Because of the pH level, Fe^{2+} ion is hydrolyzed to be insoluble coagulants of $Fe(OH)_2$ (Eq. 3a). It also can be oxidized to be Fe^{3+} and then hydrolyzed to be $Fe(OH)_3$ (Eq. 3b) [43]. Besides that, the Fe^{2+} and Fe^{3+} is also hydrolyzed to be $Fe(OH)^+$, $Fe(OH)^{2+}$ and $Fe(OH)_2^+$ that can be acting as coagulant too but they presents poor coagulative activity [37].

$$Fe^{2+} \xrightarrow{\text{hydrolysis}} Fe(OH)_2 \tag{3a}$$

$$Fe^{2+} \xrightarrow{\text{oxidation}} Fe^{3+} \xrightarrow{\text{hydrolysis}} Fe(OH)_3 \tag{3b}$$

The coagulants adsorb the pollutants (COD) to make small aggregate as shown in Eq. (4).

$$\text{Coagulant} + \text{COD} \xrightarrow{k_1} A \tag{4}$$

Because of spontaneous oxidation and hydrolysis of Fe^{2+} to be the coagulants, the rate-determining step is generation ion Fe^{2+} electrolytically [44]. Eq. (4) could be rewritten to be:

$$Fe^{2+} + \text{COD} \xrightarrow{k_1} A \tag{5}$$

After that, the flocculation occurs when the small aggregate (A) reacts each other to make the big aggregates (Eq. (6)).

$$A + A \xrightarrow{k_2} A_2 \tag{6}$$

In A_2 formation, the pollutant (COD) might be entrapped in it (Eq. (7)).

$$\text{COD} \xrightarrow{k_e} A_2 \tag{7}$$

The aggregates can be separated by sedimentation as sludge on the base (Eq. (8)). However, a part of sludge can go up as scum due to flotation by evolved H_2 during EC process (Eq. (9)).

$$A_2 \xrightarrow{k_{sl}} \text{Sludge} \tag{8}$$

$$\text{Sludge} \xrightarrow{k_{sc}} \text{Scum} \tag{9}$$

Therefore, the mechanism of EC could be summarized in Table 1.

3. Modeling

3.1. Net rate of Fe^{2+} production

Rate of Fe^{2+} ion production per second time by anode oxidation can be predicted through Faraday's law [44,45].

$$\frac{d[Fe^{2+}]}{dt} = \frac{IM_w}{zFv} \tag{10}$$

Since I is JA_s, Eq. (10) is modified to be Eq. (11)

$$\frac{d[Fe^{2+}]}{dt} = \frac{JM_wA_s}{zFv} \tag{11}$$

Rate of Fe^{2+} ion consumption for adsorbing COD is expressed by:

$$\frac{d[Fe^{2+}]}{dt} = -k_1[Fe^{2+}][COD]$$

Hence, the net rate of Fe^{2+} production is shown in Eq. (12).

$$\frac{d[Fe^{2+}]}{dt} = \frac{JM_wA_s}{zFv} - k_1[Fe^{2+}][COD] \tag{12}$$

3.2. Net rate of A production

Rate of A production from adsorption of COD on coagulant is

Table 1
The step by step of EC mechanism.

Reaction	Description
$Fe^{2+} + \text{COD} \xrightarrow{k_1} A$	Adsorption
$A + A \xrightarrow{k_2} A_2$	Flocculation
$\text{COD} \xrightarrow{k_e} A_2$	Entrapment
$A_2 \xrightarrow{k_{sl}} \text{Sludge}$	Sedimentation
$\text{Sludge} \xrightarrow{k_{sc}} \text{Scum}$	Flotation

expressed by:

$$\frac{d[A]}{dt} = k_1[Fe^{2+}][COD]$$

Rate of A consumption for producing A_2 is expressed by:

$$\frac{d[A]}{dt} = -k_2[A]^2$$

Hence, the net rate of A production is shown in Eq. (13).

$$\frac{d[A]}{dt} = k_1[Fe^{2+}][COD] - k_2[A]^2 \quad (13)$$

The A is assumed that it is formed and spontaneously decomposed into A_2, so net rate of A production is equal to zero, $\frac{d[A]}{dt} = 0$.

$$0 = k_1[Fe^{2+}][COD] - k_2[A]^2$$

$$[A]^2 = \frac{k_1}{k_2}[Fe^{2+}][COD] \quad (14)$$

3.3. Net rate of A_2 production

Rate of A_2 production from flocculation and entrapment is expressed by:

$$\frac{d[A_2]}{dt} = \frac{1}{2}k_2[A]^2 + k_e[COD]$$

Rate of decrease in A_2 to be sludge (sedimentation) is expressed by:

$$\frac{d[A_2]}{dt} = -k_{sl}[A_2]$$

Hence, the net rate of A_2 production is shown in Eq. (15).

$$\frac{d[A_2]}{dt} = \frac{1}{2}k_2[A]^2 + k_e[COD] - k_{sl}[A_2] \quad (15)$$

The A_2 is also assumed that it is formed and spontaneously decomposed into sludge, so net rate of A_2 production is equal to zero, $\frac{d[A_2]}{dt} = 0$.

$$0 = \frac{1}{2}k_2[A]^2 + k_e[COD] - k_{sl}[A_2]$$

$$[A_2] = \frac{\frac{1}{2}k_2[A]^2 + k_e[COD]}{k_{sl}} \quad (16)$$

3.4. Net rate of scum and sludge production

Rate of scum and sludge production is expressed by:

$$\frac{d[Sludge]}{dt} = k_{sl}[A_2] - k_{sc}[Sludge] \quad (17)$$

$$\frac{d[Scum]}{dt} = k_{sc}[Sludge] \quad (18)$$

Substituting Eq. (14) and (16) to Eq. (17) to get Eq. (19)

$$\frac{d[Sludge]}{dt} = \frac{1}{2}k_1[Fe^{2+}][COD] + k_e[COD] - k_{sc}[Sludge] \quad (19)$$

3.5. Net rate of decrease in COD through adsorption and entrapment

$$\frac{d[COD]}{dt} = -k_1[Fe^{2+}][COD] - k_e[COD] \quad (20)$$

Therefore, the net rate for all components is shown in Table 2.

4. Methods

4.1. Vinasse

Vinasse was collected from PT. Madukismo located in Yogyakarta, Indonesia. It contained COD, total dissolved Fe and power of Hydrogen (pH) of 100.16 ± 0.29 g L^{-1}, 38.79 ± 0.09 mg L^{-1} and 4.35 ± 0.05 respectively.

4.2. Experimental set up

Beaker glass with volume of 1 L was used as EC batch reactor. Volume of vinasse treated in this study was 1 L. The iron plats with dimension of length, width and thickness of 20 cm, 3 cm and 3 mm were used as electrodes. The dimension of the plats immersed in vinasse was 9.5 cm, 3 cm and 3 mm (active surface (A_s) of 28.5 cm^2). Therefore, the ratio of $\frac{A_s}{v}$ was 28.5 cm^2 L^{-1}. The distance of electrodes was 5.5 cm. Power DC supply (Long Wei, Series of LW-K3010D, 0 − 30 V, 0–10 A) was used as electrical current source. The agitation speed was maintained to be 200 rpm. Fig. 2 shows the experimental set up in this study.

4.3. Experimental design and procedures

Before used, the electrodes were soaked in HCl 5 %v/v solution for 15 min. After that, the electrodes were rinsed using distilled water and then weighted [25]. The initial pH of vinasse was varied to be 4.35 ± 0.05, 5.00 ± 0.00 and 6.00 ± 0.00 by using NaOH (technical grade). Voltage was maintained on 10 V. The EC process was carried out for 60 min (3600 s) with duplicate of experiments (experiment a and b). During process, the current (I, Ampere) was recorded per 10 min (600 s). Since the A_s was assumed to be constant (28.5 cm^2), the current density (J, Ampere cm^{-2}) was calculated with formula of I/28.5. The change of J during process was discussed in point of Results and Discussions. Every 600 s, the scum produced on the surface of vinasse was taken. Furthermore, it was dried under temperature of 105 − 110 °C and weighted. Then, the pH was monitored using a digital pH meter (model ATC 2011) every 600 s. The solution temperature was measured by using a mercury thermometer. Furthermore, the solution sample was taken as much as 10 − 20 mL and then placed in reaction tube for settling as long as 24 h. After settling, the supernatants were taken for COD and total dissolved Fe analysis. The COD analysis was conducted through Open Reflux and Titration Method of SNI 06–6989.15-2004. The total dissolved Fe in solution was determined in Badan Tenaga Nuklir Nasional (BATAN) by using Atomic Absorption Spectroscopy (AAS). Before the analysis of dissolved Fe, the sample was filtered by using the Whatman 42. The measured total dissolved Fe was assumed that it represented the amount of Fe^{2+} ions in solution. After the EC process, the sacrificial electrode (anode) was rinsed using distilled water and weighted. The sludge mass produced during EC was calculated by using Eq. (21). Meanwhile, the conductivy of solution during process was determined using Eq. (22) [46].

$$Sludge\ mass\ (t) + Scum\ mass\ (t) = removed\ COD\ mass\ (t) + removed\ total\ dissolved\ Fe\ mass\ (t) \quad (21)$$

Table 2
Total mass balance for modeling.

Rate	Equation
$\frac{d[COD]}{dt}$	$-k_1[Fe^{2+}][COD] - k_e[COD]$
$\frac{d[Fe^{2+}]}{dt}$	$\frac{JM_W A_s}{zFv} - k_1[Fe^{2+}][COD]$
$\frac{d[Sludge]}{dt}$	$\frac{1}{2}k_1[Fe^{2+}][COD] + k_e[COD] - k_{sc}[Sludge]$
$\frac{d[Scum]}{dt}$	$k_{sc}[Sludge]$

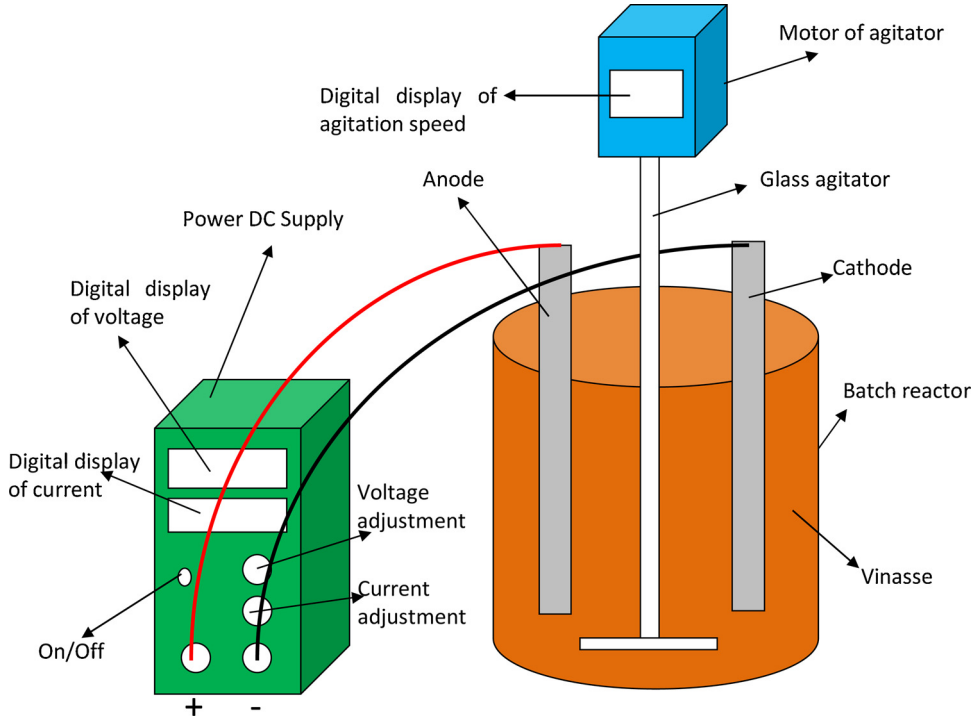

Fig. 2. Experimental set up.

Table 3
Experimental data during EC process at variation of initial pH.

pH of 4.35 ± 0.05								
Time (second)	Current (A)	pH	Temperature (°C)	Scum (g L^{-1})	Weight loss of anode (g)	COD (g L^{-1})	Conductivity (μS cm^{-1})	Total dissolved Fe (mg L^{-1})
0	2.38 ± 0.00^{a,b}	4.35 ± 0.05 ^{a,b}	28.45 ± 0.45 ^{a,b}	0.00 ± 0.00 ^{a,b}	0.00 ± 0.00 ^{a,b}	100.16 ± 0.29 ^{a,b}	45833.33 ± 96.49 ^{a,b}	38.79 ± 0.09^{b}
600	2.52 ± 0.04 ^{a,b}	4.45 ± 0.05 ^{a,b}	30.75 ± 0.75 ^{a,b}	0.21 ± 0.18 ^{a,b}	Na	98.88 ^{a}	48631.58 ± 771.93 ^{a,b}	Na
1200	2.62 ± 0.04 ^{a,b}	4.50 ± 0.00 ^{a,b}	33.75 ± 0.75 ^{a,b}	0.37 ± 0.33 ^{a,b}	Na	97.65 ± 0.67 ^{a,b}	50561.40 ± 771.93 ^{a,b}	312.87 ± 3.93^{b}
1800	2.65 ± 0.10 ^{a,b}	4.60 ± 0.00 ^{a,b}	35.65 ± 1.15 ^{a,b}	0.56 ± 0.48 ^{a,b}	Na	96.95 ± 1.93 ^{a,b}	51140.35 ± 1929.82 ^{a,b}	Na
2400	2.68 ± 0.13 ^{a,b}	4.65 ± 0.05 ^{a,b}	37.90 ± 0.90 ^{a,b}	0.74 ± 0.62 ^{a,b}	Na	96.66 ± 2.22 ^{a,b}	51719.30 ± 2508.77 ^{a,b}	642.83 ± 8.59^{b}
3000	2.72 ± 0.12 ^{a,b}	4.80 ± 0.00 ^{a,b}	39.20 ± 1.20 ^{a,b}	0.83 ± 0.68 ^{a,b}	Na	96.87 ± 0.10 ^{a,b}	52394.74 ± 2219.30 ^{a,b}	Na
3600	2.72 ± 0.11 ^{a,b}	4.90 ± 0.00 ^{a,b}	40.45 ± 1.45 ^{a,b}	0.92 ± 0.74 ^{a,b}	−2.89 ± 0.02 ^{a,b}	95.33 ± 1.65 ^{a,b}	52491.23 ± 2122.81 ^{a,b}	1147.95 ± 2.02^{b}
pH of 5.00 ± 0.00								
Time (second)	Current (A)	pH	Temperature (°C)	Scum (g L^{-1})	Weight loss of anode (g)	COD (g L^{-1})	Conductivity (μS cm^{-1})	Total dissolved Fe (mg L^{-1})
0	2.66 ± 0.23^{a,b}	5.00 ± 0.00 ^{a,b}	29.00 ± 0.00 ^{a,b}	0.00 ± 0.00 ^{a,b}	0.00 ± 0.00 ^{a,b}	100.16 ± 0.29 ^{a,b}	51236.84 ± 4342.11 ^{a,b}	38.79 ± 0.09^{b}
600	2.80 ± 0.22 ^{a,b}	5.10 ± 0.10 ^{a,b}	32.00 ± 0.00 ^{a,b}	0.41 ± 0.19 ^{a,b}	Na	96.31 ± 1.09 ^{a,b}	54035.09 ± 4245.61 ^{a,b}	Na
1200	2.90 ± 0.28 ^{a,b}	5.20 ± 0.10 ^{a,b}	34.75 ± 0.25 ^{a,b}	0.80 ± 0.25 ^{a,b}	Na	93.79 ± 1.43 ^{a,b}	55868.42 ± 5307.02 ^{a,b}	296.26 ± 0.56^{b}
1800	2.94 ± 0.29 ^{a,b}	5.30 ± 0.10 ^{a,b}	36.90 ± 0.10 ^{a,b}	1.29 ± 0.54 ^{a,b}	Na	92.86 ± 0.50 ^{a,b}	56640.35 ± 5500.00 ^{a,b}	Na
2400	2.94 ± 0.29 ^{a,b}	5.45 ± 0.15 ^{a,b}	38.75 ± 0.25 ^{a,b}	2.08 ± 1.11 ^{a,b}	Na	92.63 ± 0.27 ^{a,b}	56640.35 ± 5500.00 ^{a,b}	631.86 ± 2.83^{b}
3000	2.91 ± 0.26 ^{a,b}	5.60 ± 0.20 ^{a,b}	40.00 ± 0.00 ^{a,b}	3.19 ± 1.76 ^{a,b}	Na	91.79 ± 1.11 ^{a,b}	56061.40 ± 4921.05 ^{a,b}	Na
3600	2.85 ± 0.26 ^{a,b}	5.85 ± 0.25 ^{a,b}	41.25 ± 0.25 ^{a,b}	4.54 ± 2.15 ^{a,b}	−3.00 ± 0.19 ^{a,b}	91.56 ± 0.88 ^{a,b}	54903.51 ± 4921.05 ^{a,b}	1018.80 ± 2.03^{b}
pH of 6.00 ± 0.00								
Time (second)	Current (A)	pH	Temperature (°C)	Scum (g L^{-1})	Weight loss of anode (g)	COD (g L^{-1})	Conductivity (μS cm^{-1})	Total dissolved Fe (mg L^{-1})
0	2.98 ± 0.18^{a,b}	6.00 ± 0.00 ^{a,b}	29.75 ± 0.75 ^{a,b}	0.00 ± 0.00 ^{a,b}	0.00 ± 0.00 ^{a,b}	100.16 ± 0.29 ^{a,b}	57412.28 ± 3377.19 ^{a,b}	38.79 ± 0.09^{b}
600	2.91 ± 0.28 ^{a,b}	6.15 ± 0.05 ^{a,b}	33.00 ± 1.00 ^{a,b}	1.59 ± 0.72 ^{a,b}	Na	96.19 ^{a}	56157.89 ± 5403.51 ^{a,b}	Na
1200	2.81 ± 0.34 ^{a,b}	6.55 ± 0.05 ^{a,b}	35.55 ± 0.55 ^{a,b}	3.55 ± 0.98 ^{a,b}	Na	91.46 ^{a}	54228.07 ± 6561.40 ^{a,b}	229.50 ± 3.24^{b}
1800	2.76 ± 0.41 ^{a,b}	7.05 ± 0.25 ^{a,b}	37.25 ± 1.25 ^{a,b}	5.41 ± 1.04 ^{a,b}	Na	91.46 ^{a}	53166.67 ± 7815.79 ^{a,b}	Na
2400	2.62 ± 0.44 ^{a,b}	7.25 ± 0.35 ^{a,b}	38.50 ± 1.50 ^{a,b}	7.19 ± 1.26 ^{a,b}	Na	90.71 ^{a}	50561.40 ± 8491.23 ^{a,b}	546.36 ± 0.83^{b}
3000	2.32 ± 0.37 ^{a,b}	7.40 ± 0.30 ^{a,b}	39.50 ± 1.50 ^{a,b}	9.09 ± 1.52 ^{a,b}	Na	88.46 ± 3.00 ^{a}	44771.93 ± 7140.35 ^{a,b}	Na
3600	2.02 ± 0.25 ^{a,b}	7.50 ± 0.20 ^{a,b}	40.00 ± 2.00 ^{a,b}	10.92 ± 1.89 ^{a,b}	−2.83 ± 0.44 ^{a,b}	86.21 ± 2.25 ^{a}	38885.96 ± 4921.05 ^{a,b}	864.09 ± 0.46^{b}

Remarks: Na, not analyzed; superscript a = data obtained from experiment a; superscript b = data obtained from experiment b; superscript a,b = data obtained from experiment a,b.

$$\kappa = \frac{Id}{VA_s}10^6 \quad (22)$$

4.4. Kinetic analysis

In this study, the measured data obtained during EC process were COD, total dissolved Fe in solution, scum and sludge. Furthermore, the data was used to build a mechanistic model. Furthermore, the error was calculated by using Eq. (23).

$$Error = \sum_{i=1}^{n}\left(\frac{measured\ data - predicted\ data}{measured\ data}\right)^2 \quad (23)$$

4.5. Operating cost

The operating cost is an important term in EC process. According to Ozyonar and Karagozoglu [47], the operating cost consisted of energy, electrode, and chemical cost. Hence, calculation of operating cost (IDR L^{-1}) was expressed in Eq. (24).

$$\frac{d[OperatingCost]}{dt} = a\frac{d[EnC]}{dt} + b\frac{d[ElC]}{dt} + c\,ChC \quad (24)$$

Unit prices of a, b and c are as follows prices of electrical energy, electrode materials and chemicals. The electrical energy price for middle scale industrial use was estimated as 1115 IDR kWh^{-1} (kilowatt hour) or 30.97 × 10^{-5} IDR Ws^{-1} (watt second). The iron material price was estimated as 20,000 IDR kg^{-1} or 20 IDR g^{-1}. The chemical price for technical grade NaOH (flake) was estimated as 16,000 IDR kg^{-1}. The *EnC* (Energy Consumption) and *ElC* (Electrode Consumption) were calculated using Eq. (25) [48] and Eq. (26) [49] respectively.

$$\frac{d[EnC]}{dt} = \frac{VI}{\nu} \quad (25)$$

$$\frac{d[ElC]}{dt} = \frac{JM_wA_s}{zFv} \quad (26)$$

5. Results and discussions

5.1. Current density profile during EC

The current was monitored and presented in Table 3. Furthermore, the current density (J, Ampere cm^{-2}) was calculated with formula of I/A_s in which the A_s was assumed to be constant (28.5 cm^2). The change of J during process was shown in Fig. 3. In this study, the voltage was maintained to be constant (10 V). Thus, the change of current density was caused by the change of solution conductivity in which the higher the conductivity caused the higher the current density. The solution conductivity was also shown in Table 3.

Electrodissolution of Fe^{2+} increased the conductivity. Meanwhile when the coagulants adsorbed the pollutants and they were removed by sedimentation or flotation, the conductivity of solution decreased. At initial pH of 4.35, the current density increased slowly from beginning to the end of process. That means, the electrodissolution rate of Fe^{2+} and removal rate of COD were slow but the latter was slower. At initial pH of 5.00, current density increased from beginning until second 1800, after that it decreased. At range of second 0–1800, the electrodissolution rate of Fe^{2+} was higher than removal rate of COD. Meanwhile at range of second 1800–3600, the electrodissolution rate of Fe^{2+} was lower than removal rate of COD. At initial pH of 6.00, current density decreased until the end of process. Thus, commonly, the electrodissolution rate of Fe^{2+} was lower than removal rate of COD at initial pH of 6.00. During EC process, the solution temperature changed because of the current supplied to the solution and electrolysis time [50]. The temperature profile was same for all variables (Table 3) in which initial temperature of 28.45–29.75 °C was to be final temperature of 40.00–41.25 °C.

5.2. Comparison between measured and predicted electrode consumption

During EC process, the anode (Fe) is oxidized to be Fe^{z+} ion. The z can be 2 (Fe^{2+}, ferrous) or 3 (Fe^{3+}, ferric). Some authors believed that the Fe^{2+} is produced from electrolysis of anode [51,52], however the others believed that Fe^{3+} ion is produced directly during EC [53,54]. The value of z is important to be determined because it is directly connected to the proposed mechanistic model and operating cost calculation.

To find the appropriate z value, the electrode (anode) consumption during EC was predicted by using Eq. (26) with $z = 2$ and $z = 3$. Furthermore, the predicted electrode consumption was compared with the measured data. Comparison between measured and predicted electrode consumption is shown in Fig. 4. Based on the Fig. 4, the calculation using $z = 2$ gave much better prediction than $z = 3$. That means electrodissolution of anode in this study resulted Fe^{2+} ion. Thus, $z = 2$ was used in the mechanistic model and operating cost calculation. Lakshmanan et al. [43] also reported the same conclusion that Fe^{2+} was generated at iron anode during EC, not Fe^{3+}. The Fe^{3+} ion might be formatted from oxidation of Fe^{2+} because of the presence of dissolved oxygen and increasing in pH [43]. Therefore, Eq. (1) to (5) could be accepted.

5.3. pH, COD and total dissolved Fe profile during EC

The profile of pH and COD during EC process is shown in Table 3. During the process, the H_2O was reduced to be OH^- ion and H_2 gas. Accumulation of OH^- increased the pH of solution. For initial pH of 4.35 ± 0.05, 5.00 ± 0.00, 6.00 ± 0.00, the final pH was to be 4.90 ± 0.00, 5.85 ± 0.25, 7.50 ± 0.20 respectively. The pH level influences the iron species in solution. The higher the pH level, the more the dose of main coagulants of ($Fe(OH)_2$ and $Fe(OH)_3$) presenting in the solution. At initial pH of 4.35, solution pH changed in range of 4.35–4.90 during process. At that range, iron was in form of Fe^{2+}, $Fe(OH)_2$, $Fe(OH)_2^+$ and $Fe(OH)_3$ [37]. The $Fe(OH)_2$ and $Fe(OH)_3$ was coagulants responding in COD removal. The value of COD removal at initial pH of 4.35 was very low (4.83 %) because the main coagulant presented in low concentration.

For initial pH of 5.00 ± 0.00, the pH increased from 5.00 to 5.85. At that range, the amount of Fe^{2+} decreased, while the amount of Fe $(OH)_2^+$, $Fe(OH)_3$ and $Fe(OH)_2$ increased [37]. As consequence, the COD removal at initial pH of 5.00 ± 0.00 was higher (8.59 %) than that at initial pH of 4.35 ± 0.05 (4.83 %). The highest COD removal (13.93 %) was obtained at initial pH of 6.00 ± 0.00. At that variable, pH increased from 6.00 to 7.50, so that the amount of Fe^{2+} ion decreased and the main coagulants of $Fe(OH)_3$ and $Fe(OH)_2$ were dominant in the solution [37]. The coagulants adsorbed the pollutants easily

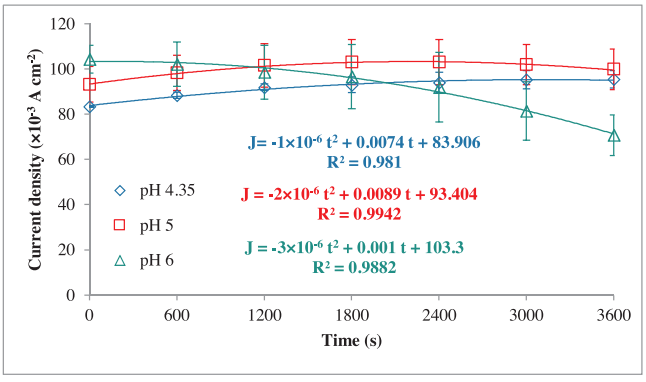

Fig. 3. Current density profile at variation of initial pH during EC.

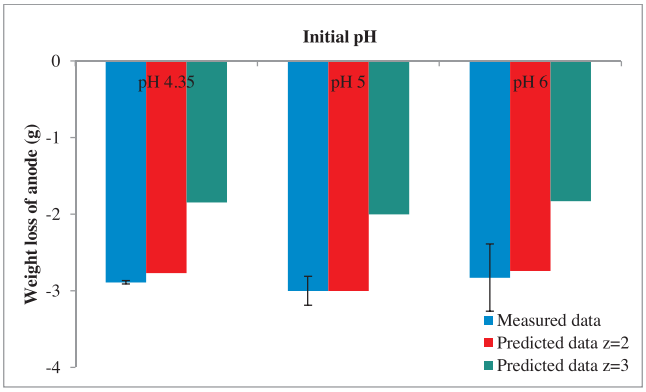

Fig. 4. Weight loss of anode after EC for 3600 s.

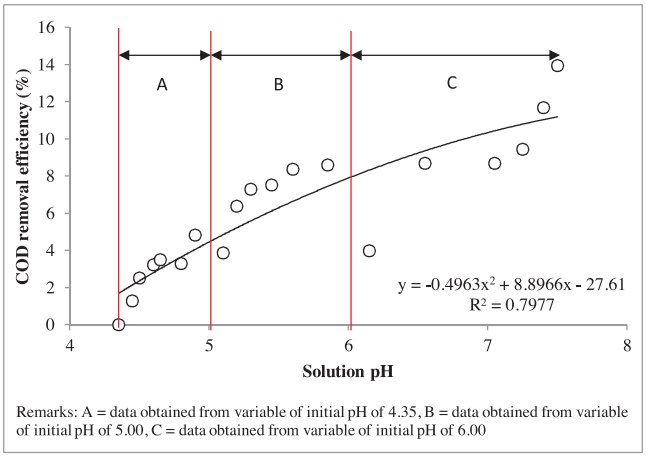

Fig. 5. The mechanism of solution pH on the COD removal efficiency.

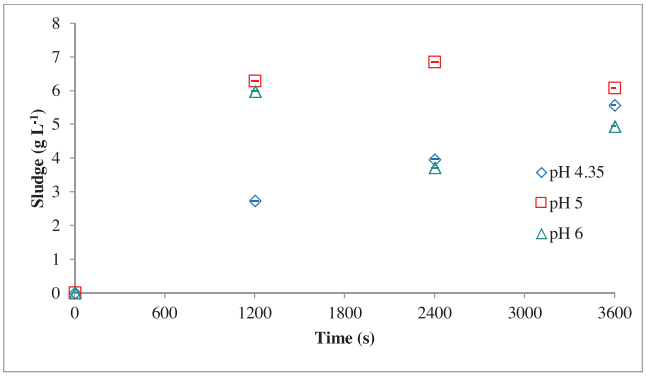

Fig. 6. Sludge production at variation of initial pH during EC.

so the COD removal was higher than the others. Demirbas and Kobya [30] also reported the same results with this study. For Fe electrode, increasing initial pH from 3 to 7 could increase COD removal from 60 to 90 %. At neutral pH, gelatinous metal coagulant was released in large amount in solution [25,55].

During EC process, the solution pH changed. Thus, correlation between the mechanism of pH and COD removal efficiency was interesting to be studied. The COD removal efficiency was calculated by Eq. (27). The correlation is shown in Fig. 5.

$$COD\ removal\ efficiency(t)(\%) = \frac{initial\ COD - COD(t)}{initial\ COD} \times 100\% \quad (27)$$

Based on Fig. 5, increase in solution pH caused increase in COD removal efficiency. It had correlation with iron species in solution. The higher the solution pH, the more the coagulants ($Fe(OH)_2$ and $Fe(OH)_3$) were formed [37]. Then, they adsorbed the pollutant so the COD removal efficiency was obtained in higher solution pH. However, the COD removal efficiency will decrease when the solution pH more than 8.00 [30,42]. In this study, initial pH of 6.00 showed the good phenomena of pH change where it changed from 6.00 to 7.50. The pH range was good for formation of coagulants. If initial pH of neutral is conducted, the solution pH range might be from 7.00 to more than 8.00. That range is still good for formation of the coagulants so initial pH of 7.00 will give the same result of COD removal efficiency with initial pH of 6.00. Furthermore, if initial pH of alkaline (pH of 8.00–14.00) is conducted, the COD removal efficiency decreases because the main coagulants will be dissolved again to be species of $Fe(OH)^+$, $Fe(OH)_3^-$ and $Fe(OH)_4^-$.

The pH level affected the form of Fe species in solution. Coagulants ($Fe(OH)_3$ and $Fe(OH)_2$) were assumed to be sludge and scum completely. Furthermore, the Fe^{3+} ion that might be formed because of oxidation and hydrolysis of Fe^{2+} was completely become $Fe(OH)_3$. Hence, Fe^{2+} remained dominantly in solution. In assumption, the remaining total dissolved Fe concentration measured by AAS was equal to the remaining Fe^{2+} concentration in solution. The remaining total dissolved Fe in solution is measured and shown in Table 3.

As explanation above, the higher the pH level, the more the Fe^{2+} ion was to be coagulants; consequently the more the COD was removed. There is good correlation between COD and total dissolved Fe profile during EC where the higher the remaining COD level, the higher the remaining total dissolved Fe. Based on Table 3, anode weight was decreased as much as -2.89 ± 0.02, -3.00 ± 0.19 and -2.83 ± 0.44 g for initial pH of 4.35, 5.00 and 6.00. That means the lost weight of anode was dissolved in solution. Because the raw vinasse contained total dissolved Fe of 38.79 ± 0.09 mg L^{-1}, the total dissolved Fe in vinasse was to be 2928.79, 3038.79 and 2868.79 mg L^{-1} for initial pH of 4.35, 5.00 and 6.00 respectively. After EC for 3600 s, the remaining total dissolved Fe at initial pH of 4.35, 5.00 and 6.00 was 1147.95 ± 2.02, 1018.80 ± 2.03 and 864.09 ± 0.46 mg L^{-1} respectively (Table 3). In other words, the removed total dissolved Fe in solution, which became coagulants adsorbing pollutants to form sludge and scum, at initial pH of 6.00 (2004.70 mg L^{-1} or 69.88 %) was higher than that at initial pH of 4.35 (1780.84 mg L^{-1} or 60.80 % and pH 5.00 (2019.99 mg L^{-1} or 66.47 %).

Alkalinity could be measured by Eq. (28) [56]. In this study, pH of raw vinasse was 4.35. The NaOH was added to adjust pH of vinasse to be 5.00 and 6.00. During EC process, the OH^- ion was produced by reduction at cathode. Hence, in this study, the alkalinity change in vinasse mainly depended on OH^- concentration. Therefore, Eq. (28) was rearranged to be Eq. (29). The OH^- concentration was predicted by $exp(pH - 14)$.

$$Alkalinity = [HCO_3^-] + 2[CO_3^{2-}] + [OH^-] - [H^+] \quad (28)$$

$$Alkalinity = [OH^-] \quad (29)$$

During EC process, the pH of vinasse increased (see Table 3). It showed the alkalinity of vinasse increased where the higher the pH of vinasse, the higher the alkalinity of vinasse would be. The Fe^{2+} ion, that was produced by oxidation at anode, consumed the OH to form coagulant of $Fe(OH)_2$. Hence, the higher OH^- concentration, the more $Fe(OH)_2$ produced would be. Therefore, initial pH of 6 resulted more Fe $(OH)_2$ amount than the ones of the two others with lower initial pH.

5.4. Scum and sludge profile during EC

The pollutants adsorbed by coagulants either go to base as sludge or go to surface as scum due to evolved H_2. The scum production during EC is presented in Table 3. The production rate of scum at initial pH of 6.00 was higher than that at initial pH of 4.35 and 5.00. Initial pH of 6 produced more coagulants than the others, so aggregates were easy to be formed. Furthermore, the aggregates were to be the bigger due to the

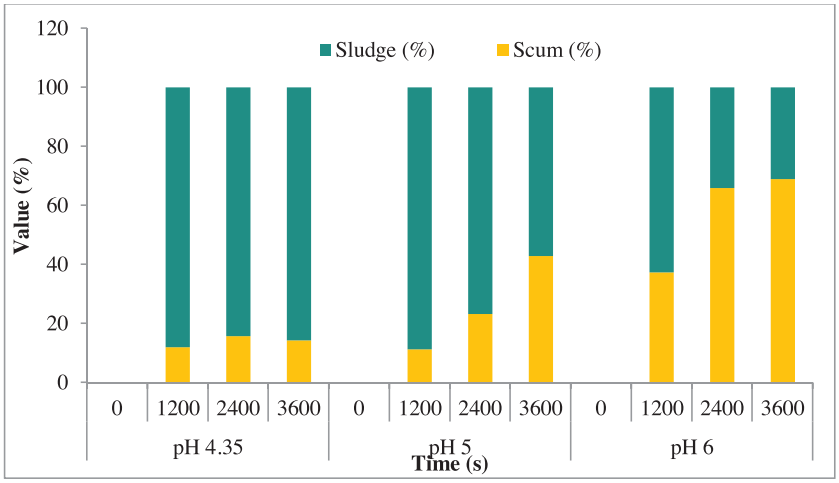

Fig. 7. Percentage of sludge and scum during EC process at various initial pH.

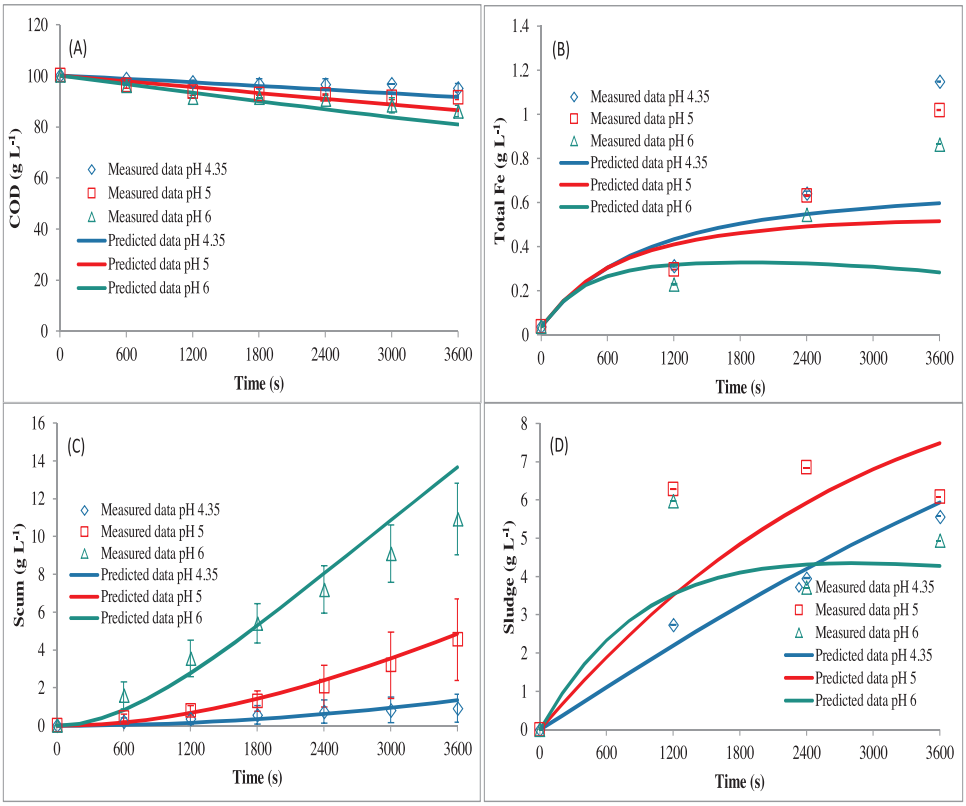

Fig. 8. Plotting between measured and predicted data using the mechanistic model (A) COD concentration, (B) total dissolved Fe concentration, (C) scum concentration, (D) sludge concentration.

Table 4
Kinetic constants obtained from simulation for EC process at various initial pH with ratio of $A_s/v = 28.5\ cm^2\ L^{-1}$, working volume of 1 L and electrode distance of 5.5 cm.

Kinetic constants	Initial pH		
	4.35	5.00	6.00
k_1 (L g^{-1} sec^{-1})	1.42×10^{-5}	1.83×10^{-5}	2.65×10^{-5}
k_{sc} (sec^{-1})	1.19×10^{-4}	3.02×10^{-4}	1.10×10^{-3}
k_e (sec^{-1})	1.79×10^{-5}	3.30×10^{-5}	5.14×10^{-5}
Error	1.8442	1.1271	1.3696

flocculation. Because of its big size, they were easy to go to surface as scum.

The sludge during EC was predicted by using Eq. (21) and then shown in Fig. 6. Furthermore, Fig. 7 showed the how much (%) the aggregates separated by sedimentation or by flotation. Commonly, the %sludge decreased and %scum increased during EC for all variation of initial pH. The solution pH increased during EC (Table 3). The higher the pH, the more the coagulants were formed. The coagulants adsorbed the pollutants. In conclusion, the longer the electrolysis time, the more and the bigger the aggregates in solution. Because of the big size (or the large contact area), the aggregates are easier to be separated by flotation. After EC for 3600 s, the %scum on initial pH of 4.35, 5.00 and 6.00 was 14.23, 42.78 and 68.86 % respectively. It showed that initial pH of

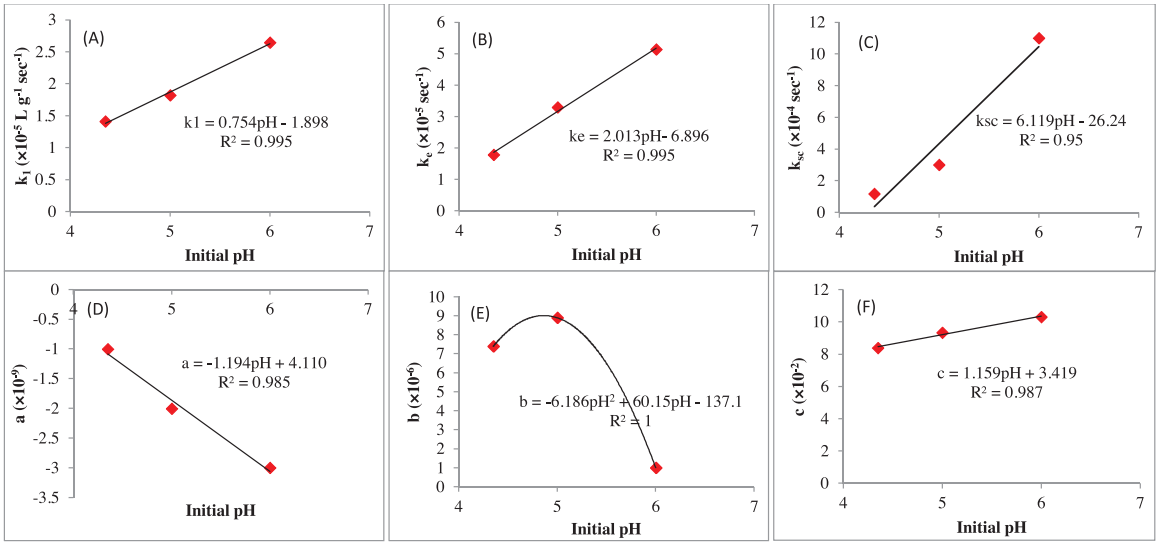

Fig. 9. Correlation between initial pH and kinetic constants of (A) k_1, (B) k_e, (C) k_{sc}, (D) a, (E) b, (F) c.

Table 5
Operational cost EC process after 3600 s.

Initial pH	Electrode cost (IDR L^{-1})	Energy cost (IDR L^{-1})	Chemical cost (IDR L^{-1})	Total cost (IDR L^{-1})	Removed COD (g L^{-1})	Removed COD/Total cost (g IDR^{-1})
4.35	55.32	29.52	0	84.84	4.83	0.0570
5.00	60.01	32.02	77.95	169.98	8.60	0.0506
6.00	54.83	29.26	135.29	219.39	13.95	0.0636

6.00 produced more big aggregates than the others.

5.5. Modeling

The mechanistic model was successfully applied in this study. Plotting between measured and predicted data is shown in Fig. 8 and the kinetic constant values are presented in Table 4. The value of k_1 represented the reaction rate constant of adsorption of pollutants (COD) on coagulants. The k_1 value of initial pH of 6.00 (2.65×10^{-5} L g^{-1} sec^{-1}) was higher than the others (1.42×10^{-5} and 1.83×10^{-5} L g^{-1} sec^{-1}). As explanation above, initial pH of 6.00 resulted more coagulants than initial pH of 4.35 and 5.00, so the adsorption rate was faster.

Furthermore, the k_e value at initial pH of 6.00 was also higher than the others (Table 4). Kinetic constant of k_e represented the rate of entrapment when the bigger aggregate was formed. Thus, the more the aggregate in system, the easier the big aggregate was formed, so the easier the pollutant was entrapped. The rate of entrapment of pollutants at initial pH of 6.00 was the fastest because it produced the most coagulants of all variables.

Increasing initial pH from 4.35 to 6.00 increased the k_{sc} value. That phenomena showed that the higher the pH condition, the more the pollutants would be removed through flotation. Scum were easily produced at initial pH of 6 because aggregates were easy to be formed.

5.6. Development of mathematical equations to predict the EC performance in the other initial pH

The NaOH (technical grade) was added to adjust initial pH of vinasse to be 5.00 and 6.00 from the origin pH of 4.35. The addition of NaOH caused the increasing of electrolyte in vinasse. Hence, the initial current density was difference for all initial pH although the voltage was kept constant in 10 V. Current density profile during EC is shown in Fig. 3. The profile was figured through polynomial with degree of 2 with common formula $J = at^2 + bt + c$. The constant value of a, b and c is shown in Fig. 3. Hence, it is important to predict correlation between initial pH with value of a, b and c. After that, the profile of current density during EC for other initial pH with range 4.35–6.00 can be predicted. The plotting between constants of a, b, c and initial pH is presented in Fig. 9. The EC process in this study was influenced by initial pH. Furthermore, the mathematical equation expressing the correlation between initial pH on kinetic constants of k_1, k_{sc}, k_e was built (see Fig. 9). By using equations in Fig. 9, EC performance with another initial pH with range 4.35–6.00 could be predicted.

5.7. Operating cost

Operating cost in EC process mainly depends on electrode, energy and chemical cost. Electrode cost was predicted successfully and shown in Table 5. Variable of initial pH of 5.00 needed higher electrode cost than initial pH of 4.35 and 6.00. The higher the current in EC, the more the electrode was to be Fe^{2+} ion in solution, so that the more the weight of electrode was needed. As consequence, the electrode cost was high. The high current in EC process also resulted the high energy cost. Furthermore, the chemical cost for all variables depended on using of NaOH for adjusting initial pH. The chemical cost for initial pH of 4.35, 5.00, 6.00 is shown in Table 5. Therefore, the total operating cost for initial pH of 4.35, 5.00 and 6.00 was 84.84, 169.98 and 219.39 IDR L^{-1} respectively. Ratio between removed COD to total cost after 3600 s for initial pH of 4.35, 5.00 and 6.00 was 0.0570, 0.0506 and 0.0636 g IDR^{-1} respectively (Table 5). Hence, initial pH of 6.00 was more effective and efficient to remove pollutants than initial pH of 4.35 and 5.00.

5.8. Comparison this study with other studies on COD removal

Comparison this study with other studies on COD removal is shown in Table 6. The COD removal efficiency in this study (13.90 %) was lower than that in study of Khandegar and Saroha [57], Asaithambi et al. [58], Aziz et al. [59], Asaithambi et al. [28] with value of 62–92.5 %. The difference was caused by that this study used very high initial

Table 6
Comparison results in this study with others.

No	Wastes	Country	COD_i (mg L^{-1})	Electrodes	Electrode distance (cm)	Current density (A m^{-2})	Temperature	Initial pH	Agitation speed (rpm)	Chemical addition	Operation time (min)	Removal efficiency (%)	References
1	Vinasse	Indonesia	100,160	irons	5.5	922.56 (average)	Room temperature	6	200	–	60	13.93	This study
2	Vinasse	Turkey	4,750	irons	0.3	200	Ambient temperature	5.15	–	0.2 M Na_2SO_4	180	14.3	[26]
3	Vinasse	India	3,360	irons	3	718	–	7.5	500	–	120	88	[57]
4	Vinasse	India	2,500	irons	1	300	Constant temperature = 30 ± 2 °C	6	–	–	240	62	[58]
5	Vinasse	Malaysia	2,000	irons	2	50	Room temperature	6	–	–	240	92.5	[59]
6	Vinasse	Malaysia	2,500	irons	3	13	Constant temperature = 35 ± 1 °C	7	100	234 mg/L H_2O_2	240	72	[28]

Remarks: COD_i, initial COD in experiment.

COD concentration (103,180 mg L^{-1}) and short operation time (60 min), while the others used low initial COD concentration (2,000–3,360 mg L^{-1}) and long operation time (120 − 240 min). That was in line with report of Fayad [46] where removal efficiency decreases with the increase in initial pollutant concentration. Furthermore, according to Garcia-Segura et al. [37], the longer the operation time, the more the pollutants can be removed from the wastes. In other side, like this study, study of Yavuz [26] showed the low COD removal efficiency (14.3 %) although Yavuz [26] used low initial COD concentration 4,750 mg L^{-1}) and long operation time of 180 min. It might be caused by that the electrode distance was too close (0.3 cm). Very close of electrode distance is not good because the movement of ions is very quick so that will prevent the formation of flocs which are required to adsorb the pollutants [27].

6. Conclusion

Initial pH of 4.35, 5.00, 6.00 showed the difference of EC performance on COD, total dissolved Fe, scum, sludge and pH profile during process. The COD removal at initial pH of 6.00 (13.93 %) was higher than that at the others (4.83–8.59 %). The remaining total dissolved Fe at initial pH of 6.00 was lower than the others. Scum and sludge production increased with increasing initial pH from 4.35 to 6.00. Furthermore, a mechanistic model was successfully built and applied in EC for vinasse waste. In the model, reactions in EC were assumed that they were adsorption, flocculation, entrapment, flotation and sedimentation. Reaction rate constants of k_1 (adsorption), k_{sc} (flotation) and k_e (entrapment) increased with increasing of initial pH from 4.35 to 6.00. Mathematical equations presenting correlation between initial pH with kinetic constants were successfully built. In operating cost calculation, ratio between removed COD to total operating cost for initial pH of 4.35, 5.00 and 6.00 was 0.0570, 0.0506 and 0.0636 g IDR^{-1} respectively.

CRediT authorship contribution statement

Iqbal Syaichurrozi: Conceptualization, Methodology, Software, Formal analysis, Investigation, Resources, Data curation, Writing - original draft, Visualization, Funding acquisition. **Sarto Sarto:** Conceptualization, Methodology, Resources, Writing - review & editing, Supervision, Project administration, Funding acquisition. **Wahyudi Budi Sediawan:** Methodology, Software, Validation, Writing - review & editing, Supervision. **Muslikhin Hidayat:** Software, Validation, Writing - review & editing, Supervision.

Declaration of Competing Interest

The authors declare that they have no known competing financial interests or personal relationships that could have appeared to influence the work reported in this paper.

Acknowledgement

The authors thank to Lembaga Pengelola Dana Pendidikan (LPDP), Kementerian Keuangan, Republik Indonesia via Beasiswa Unggulan Dosen Indonesia-Dalam Negeri (BUDI-DN) scholarship for financial support.

References

[1] D. Khatiwada, S. Silveira, Scenarios for bioethanol production in Indonesia: How can we meet mandatory blending targets? Energy 119 (2017) 351–361, https://doi.org/10.1016/j.energy.2016.12.073.

[2] I. Syaichurrozi, S. Suhirman, T. Hidayat, Effect of initial pH on anaerobic co-digestion of Salvinia molesta and rice straw for biogas production and kinetics, Biocatal. Agric. Biotechnol. 16 (2018) 594–603, https://doi.org/10.1016/j.bcab.2018.10.007.

[3] I. Syaichurrozi Budiyono, S. Sumardiono, Predicting kinetic model of biogas production and biodegradability organic materials: Biogas production from vinasse at variation of COD/N ratio, Bioresour. Technol. 149 (2013) 390–397, https://doi.org/10.1016/j.biortech.2013.09.088.
[4] J.A. Siles, I. García-García, A. Martín, M.A. Martín, Integrated ozonation and biomethanization treatments of vinasse derived from ethanol manufacturing, J. Hazard. Mater. 188 (2011) 247–253, https://doi.org/10.1016/j.jhazmat.2011.01.096.
[5] V.G. de Barros, R.M. Duda, J. da Silva Vantini, W.P. Omori, M.I.T. Ferro, R.A. de Oliveira, Improved methane production from sugarcane vinasse with filter cake in thermophilic UASB reactors, with predominance of Methanothermobacter and Methanosarcina archaea and Thermotogae bacteria, Bioresour. Technol. 244 (2017) 371–381, https://doi.org/10.1016/j.biortech.2017.07.106.
[6] K. Lutoslawki, A. Ryznar-Luty, E. Cibis, M. Krzywonos, T. Miskiewicz, Biodegradation of beet molasses vinasse by a mixed culture of microorganisms: effect of aeration conditions and pH control, J. Environ. Sci. China (China) 23 (11) (2011) 1823–1830, https://doi.org/10.1016/S1001-0742(10)60579-7.
[7] I. Budiyono, S. Syaichurrozi, Sumardiono, Effect of total solid content to biogas production rate from vinasse, Int. J. Eng. 27 (2) (2014) 177–184, https://doi.org/10.5829/idosi.ije.2014.27.02b.02.
[8] A. Sepehri, M.-H. Sarrafzadeh, Effect of nitrifiers community on fouling mitigation and nitrification efficiency in a membrane bioreactor, Chem Eng Process: Process Intensification 128 (2018) 10–18, https://doi.org/10.1016/j.cep.2018.04.006.
[9] A. Sepehri, M.-H. Sarrafzadeh, M. Avateffazeli, Interaction between Chlorella vulgaris and nitrifying-enriched activated sludge in the treatment of wastewater with low C/N ratio, J. Clean. Prod. 247 (2019) 119164, , https://doi.org/10.1016/j.jclepro.2019.119164.
[10] X. Zhang, Q. Huang, F. Deng, H. Huang, Q. Wan, M. Liu, Y. Wei, Mussel-inspired fabrication of functional materials and their environmental applications: progress and prospects, Appl. Mater. Today. 7 (2017) 222–238, https://doi.org/10.1016/j.apmt.2017.04.001.
[11] G. Zeng, L. Huang, Q. Huang, M. Liu, D. Xu, H. Huang, Z. Yang, F. Deng, X. Zhang, Y. Wei, Rapid synthesis of MoS2-PDA-Ag nanocomposites as heterogeneous catalysts and antimicrobial agents via microwave irradiation, Appl. Surf. Sci. 459 (2018) 588–595, https://doi.org/10.1016/j.apsusc.2018.07.144.
[12] Y. Liu, K. Ai, L. Lu, Polydopamine and Its Derivative Materials: Synthesis and Promising Applications in Energy, Environmental, and Biomedical Fields, Chem. Rev. 114 (9) (2014) 5057–5115, https://doi.org/10.1021/cr400407a.
[13] G. Zeng, T. Chen, L. Huang, M. Liu, R. Jiang, Q. Wan, Y. Dai, Y. Wen, X. Zhang, Y. Wei, Surface modification and drug delivery applications of MoS2 nanosheets with polymers through the combination of mussel inspired chemistry and SET-LRP, J. Taiwan. Inst. Chem. Eng. 82 (2018) 205–213, https://doi.org/10.1016/j.jtice.2017.08.025.
[14] Q. Huang, J. Zhao, M. Liu, Y. Li, J. Ruan, Q. Li, J. Tian, X. Zhu, X. Zhang, Y. Wei, Synthesis of polyacrylamide immobilized molybdenum disulfide (MoS2 @PDA@PAM) composites via mussel-inspired chemistry and surface-initiated atom transfer radical polymerization for removal of copper (II) ions, J. Taiwan. Inst. Chem. Eng. 86 (2018) 174–184, https://doi.org/10.1016/j.jtice.2017.12.027.
[15] G. Zeng, X. Liu, M. Liu, Q. Huang, D. Xu, Q. Wan, H. Huang, F. Deng, X. Zhang, Y. Wei, Facile preparation of carbon nanotubes based carboxymethyl chitosan nanocomposites through combination of mussel inspired chemistry and Michael addition reaction: characterization and improved Cu2+ removal capability, J. Taiwan. Inst. Chem. Eng. 68 (2016) 446–454, https://doi.org/10.1016/j.jtice.2016.09.008.
[16] X. Zhang, Q. Huang, M. Liu, J. Tian, G. Zeng, Z. Li, K. Wang, Q. Zhang, Q. Wan, F. Deng, Y. Wei, Preparation of amine functionalized carbon nanotubes via a bioinspired strategy and their application in Cu2+removal, Appl. Surf. Sci. 343 (2015) 19–27, https://doi.org/10.1016/j.apsusc.2015.03.081.
[17] Q. Huang, M. Liu, L. Mao, D. Xu, G. Zeng, H. Huang, R. Jiang, F. Deng, X. Zhang, Y. Wei, Surface functionalized SiO2 nanoparticles with cationic polymers via the combination of mussel inspired chemistry and surface initiated atom transfer radical polymerization: characterization and enhanced removal of organic dye, J. Colloid Interface Sci. 499 (2017) 170–179, https://doi.org/10.1016/j.jcis.2017.03.102.
[18] Q. Huang, M. Liu, J. Chen, Q. Wan, J. Tian, L. Huang, R. Jiang, Y. Wen, X. Zhang, Y. Wei, Facile preparation of MoS2 based polymer composites via mussel inspired chemistry and their high efficiency for removal of organic dyes, Appl. Surf. Sci. 419 (2017) 35–44, https://doi.org/10.1016/j.apsusc.2017.05.006.
[19] Q. Huang, J. Zhao, M. Liu, J. Chen, X. Zhu, T. Wu, J. Tian, Y. Wen, X. Zhang, Y. Wei, Preparation of polyethylene polyamine@tannic acid encapsulated MgAl-layered double hydroxide for the efficient removal of copper (II) ions from aqueous solution, J. Taiwan. Inst. Chem. Eng. 82 (2018) 92–101, https://doi.org/10.1016/j.jtice.2017.10.019.
[20] Y. Liu, H. Huang, D. Gan, L. Guo, M. Liu, J. Chen, F. Deng, N. Zhou, X. Zhang, Y. Wei, A facile strategy for preparation of magnetic graphene oxide composites and their potential for environmental adsorption, Ceram. Int. 44 (15) (2018) 18571–18577, https://doi.org/10.1016/j.ceramint.2018.07.081.
[21] Q. Huang, M. Liu, J. Zhao, J. Chen, G. Zeng, H. Huang, J. Tian, Y. Wen, X. Zhang, Y. Wei, Facile preparation of polyethylenimine-tannins coated SiO2 hybrid materials for Cu2+ removal, Appl. Surf. Sci. 427 (2018) 535–544, https://doi.org/10.1016/j.apsusc.2017.08.233.
[22] D. Gan, M. Liu, H. Huang, J. Chen, J. Dou, Y. Wen, Q. Huang, Z. Yang, X. Zhang, Y. Wei, Facile preparation of functionalized carbon nanotubes with tannins through mussel-inspired chemistry and their application in removal of methylene blue, J. Mol. Liq. 271 (2018) 246–253, https://doi.org/10.1016/j.molliq.2018.08.079.
[23] Y. Lei, Y. Cui, Q. Huang, J. Dou, D. Gan, F. Deng, M. Liu, X. Li, X. Zhang, Y. Wei, Facile preparation of sulfonic groups functionalized Mxenes for efficient removal of methylene blue, Ceram. Int. 45 (2019) 17653–17661, https://doi.org/10.1016/j.ceramint.2019.05.331.
[24] N. Kannan, G. Karthikeyan, N. Tamilselva, Comparison of treatment potential of electrocoagulation of distillery effluent with and without activated Areca catechu nut carbon, J. Hazard. Mater. B137 (2006) 1803–1809, https://doi.org/10.1016/j.jhazmat.2006.05.048.
[25] C. David, M. Arivazhagan, F. Tuvakara, Decolorization of distillery spent wash effluent by electrooxidation (EC and EF) and Fenton processes: a comparative study, Ecotoxicol. Environ. Saf. 121 (2015) 142–148, https://doi.org/10.1016/j.ecoenv.2015.04.038.
[26] Y. Yavuz, EC and EF processes for the treatment of alcohol distillery wastewater, Sep. Purif. Technol. 53 (2007) 135–140, https://doi.org/10.1016/j.seppur.2006.08.022.
[27] V. Khandegar, A.K. Saroha, Electrochemical treatment of distillery spent wash using aluminum and Iron electrodes, Chin. J. Chem. Eng. 20 (3) (2012) 439–443, https://doi.org/10.1016/S1004-9541(11)60204-8.
[28] P. Asaithambi, Baharak Sajjadi, A. Aziz, A. Raman, W. Daud, W.M.A. Bin, Performance evaluation of hybrid electrocoagulation process parameters for the treatment of distillery industrial effluent, Process Saf. Environ. Prot. 104 (2016) 406–412, https://doi.org/10.1016/j.psep.2016.09.023.
[29] J.A. Davila, F. Machuca, N. Marrianga, Treatment of vinasses by electrocoagulation–electroflotation using the Taguchi method, Electrochim. Acta 56 (2011) 7433–7436, https://doi.org/10.1016/j.electacta.2011.07.015.
[30] E. Demirbas, M. Kobya, Operating cost and treatment of metalworking fluid wastewater by chemical coagulation and electrocoagulation processes, Process Saf. Environ. Prot. 105 (2017) 79–90, https://doi.org/10.1016/j.psep.2016.10.013.
[31] M. Elazzouzi, Kh. Haboubi, M.S. Elyoubi, Electrocoagulation flocculation as a low-cost process for pollutants removal from urban wastewater, Chem. Eng. Res. Des. 117 (2017) 614–626, https://doi.org/10.1016/j.cherd.2016.11.011.
[32] B.-Y. Tak, B.-S. Tak, Y.-J. Kim, Y.-J. Park, Y.-H. Yoon, G.-H. Min, Optimization of color and COD removal from livestock wastewater by electrocoagulation process: application of Box–behnken design (BBD), J. Ind. Eng. Chem. 28 (2015) 307–315, https://doi.org/10.1016/j.jiec.2015.03.008.
[33] D. Wagle, C.-J. Lin, T. Nawaz, H.J. Shipley, Evaluation and optimization of electrocoagulation for treating Kraft paper mill wastewater, J. Environ. Chem. Eng. 8 (1) (2020) 103595, , https://doi.org/10.1016/j.jece.2019.103595.
[34] E.K. Mroczek, D. Graham, L. Bacon, Removal of arsenic and silica from geothermal fluid by electrocoagulation, J. Environ. Chem. Eng. 7 (4) (2019) 103232, , https://doi.org/10.1016/j.jece.2019.103232.
[35] M. Kobya, P.I. Omwene, Z. Ukundimana, Treatment and operating cost analysis of metalworking wastewaters by a continuous electrocoagulation reactor, J. Environ. Chem. Eng. (2019), https://doi.org/10.1016/j.jece.2019.103526.
[36] H.J. You, I.S. Han, Effects of dissolved ions and natural organic matter on electrocoagulation of As(III) in groundwater, J. Environ. Chem. Eng. 4 (1) (2016) 1008–1016, https://doi.org/10.1016/j.jece.2015.12.034.
[37] S. Garcia-Segura, M.M.S.G. Eiband, J.V. de Melo, C.A. Martínez-Huitle, Electrocoagulation and advanced electrocoagulation processes: a general review about the fundamentals, emerging applications and its association with other technologies, J. Electroanal. Chem. Lausanne (Lausanne) 801 (2017) 267–299, https://doi.org/10.1016/j.jelechem.2017.07.047.
[38] A. Mohammadi, A. Khadir, R.M.A. Tehrani, Optimization of nitrogen removal from an anaerobic digester effluent by electrocoagulation process, J. Environ. Chem. Eng. 7 (3) (2019) 103195, , https://doi.org/10.1016/j.jece.2019.103195.
[39] L. Largitte, R. Pasquier, A review of the kinetics adsorption models and their application to the adsorption of lead by an activated carbon, Chem. Eng. Res. Des. 109 (2016) 495–504, https://doi.org/10.1016/j.cherd.2016.02.006.
[40] Y.A. Ouaissa, M. Chabani, A. Amrane, A. Bensmaili, Removal of tetracycline by electrocoagulation: kinetic and isotherm modeling through adsorption, J. Environ. Chem. Eng. 2 (1) (2014) 177–184, https://doi.org/10.1016/j.jece.2013.12.009.
[41] A.G. Khorram, N. Fallah, Treatment of textile dyeing factory wastewater by electrocoagulation with low sludge settling time: optimization of operating parameters by RSM, J. Environ. Chem. Eng. 6 (1) (2018) 635–642, https://doi.org/10.1016/j.jece.2017.12.054.
[42] M.E. Olya, A. Pirkarami, Electrocoagulation for the removal of phenol and aldehyde contaminants from resin effluent, Water Sci. Technol. 68 (9) (2013) 1940–1949, https://doi.org/10.2166/wst.2013.439.
[43] D. Lakshmanan, D.A. Clifford, G. Samanta, Ferrous and Ferric Ion Generation During Iron Electrocoagulation, Environ. Sci. Technol. 43 (2009) 3853–3859, https://doi.org/10.1021/es8036669.
[44] J.N. Hakizimana, B. Gourich, M. Chafi, Y. Stiriba, C. Vial, P. Drogui, J. Naja, Electrocoagulation process in water treatment: a review of electrocoagulation modeling approaches, Desalination 404 (2017) 1–21, https://doi.org/10.1016/j.desal.2016.10.011.
[45] M. Dolati, A.A. Aghapour, H. Khorsandi, S. Karimzade, Boron removal from aqueous solutions by electrocoagulation at low concentrations, J. Environ. Chem. Eng. 5 (5) (2017) 5150–5156, https://doi.org/10.1016/j.jece.2017.09.055.
[46] N. Fayad, The Application of Electrocoagulation Process for Wastewater Treatment and for the Separation and Purification of Biological Media, Chemical and Process Engineering, Université Clermont Auvergne, 2017 Doctoral Thesis.
[47] F. Ozyonar, B. Karagozoglu, Treatment of pretreated coke wastewater by electrocoagulation and electrochemical peroxidation processes, Sep. Purif. Technol. 150 (2015) 268–277, https://doi.org/10.1016/j.seppur.2015.07.011.
[48] H. Singh, B.K. Mishra, Assessment of kinetics behavior of electrocoagulation process for the removal of suspended solids and metals from synthetic water, Int. J. Civ. Struct. Environ. Infrastruct. Eng. Res. Dev. 22 (2) (2017) 141–148, https://doi.org/

10.4491/eer.2016.029.
[49] M. Kobya, F. Ozyonar, E. Demirbas, E. Sik, M.S. Oncel, Arsenic removal from groundwater of Sivas-Şarkişla Plain, Turkey by electrocoagulation process: comparing with iron plate and ball electrodes, J. Environ. Chem. Eng. 3 (2) (2015) 1096–1106, https://doi.org/10.1016/j.jece.2015.04.014.
[50] S.O. Giwa, K. Polat, H. Hapoglu, The effects of operating parameters on temperature and electrode dissolution in electrocoagulation treatment of petrochemical wastewater, Int. J. Eng. Res. Technol. 1 (10) (2012) 1–9.
[51] R. Parga, D.L. Cocke, V. Valverde, Characterization of electrocoagulation for removal of chromium and arsenic, Chem. Eng. Technol. 28 (5) (2005) 605–612, https://doi.org/10.1002/ceat.200407035.
[52] M.Y. Mollah, R. Schennach, J.R. Parga, D.L. Cocke, Electrocoagulation (EC) - science and applications, J. Hazard. Mater. 84 (1) (2001) 29–41, https://doi.org/10.1016/S0304-3894(01)00176-5.
[53] M. Kobya, E. Senturk, M. Bayramoglu, Treatment of poultry slaughterhouse wastewaters by electrocoagulation, J. Hazard. Mater. 133 (1) (2006) 172–176, https://doi.org/10.1016/j.jhazmat.2005.10.007.
[54] M.Y. Mollah, P.G. Morkovsky, A.G. Gomes, M. Kesmez, J. Parga, Fundamentals, Present and Future Perspectives of Electrocoagulation, J. Hazard. Mater. 114 (1-3) (2004) 199–210, https://doi.org/10.1016/j.jhazmat.2004.08.009.
[55] E. Nariyan, A. Aghababaei, M. Sillanpää, Removal of pharmaceutical from water with an electrocoagulation process; effect of various parameters and studies of isotherm and kinetic, Sep. Purif. Technol. 188 (2017) 266–281, https://doi.org/10.1016/j.seppur.2017.07.031.
[56] S.E. Manahan, Water Chemistry: Green Science and Technology of Nature's Most Renewable Resource, CRC Press, Taylor & Francis Group, 2010.
[57] V. Khandegar, A.K. Saroha, Electrocoagulation of distillery spentwash for complete organic reduction, Int. J. Chemtech Res. 5 (2) (2013) 712–718.
[58] P. Asaithambi, M. Susree, R. Saravanathamizhan, M. Matheswaran, Ozone assisted electrocoagulation for the treatment of distillery effluent, Desalination 297 (2012) 1–7, https://doi.org/10.1016/j.desal.2012.04.011.
[59] A.R.A. Aziz, P. Asaithambi, W.M.A.B.W. Daud, Combination of electrocoagulation with advanced oxidation processes for the treatment of distillery industrial effluent, Process Saf. Environ. Prot. 99 (2016) 227–235, https://doi.org/10.1016/j.psep.2015.11.010.